An Investigation of Stall Inception in Centrifugal Compressor Vaned Diffusers

Proceedings of ASME Turbo Expo 2011
GT2011
June 6-10, 2011, Vancouver, British Columbia, Canada

GT2011-46332

AN INVESTIGATION OF STALL INCEPTION IN CENTRIFUGAL COMPRESSOR VANED DIFFUSERS

J.N. Everitt and Z.S. Spakovszky
Gas Turbine Laboratory
Massachusetts Institute of Technology
Cambridge, MA, 02139

ABSTRACT

In compression systems the stable operating range is limited by rotating stall and/or surge. Two distinct types of stall precursors can be observed prior to full scale instability: the development of long-wavelength modal waves or a short-wavelength, three-dimensional flow breakdown (so-called "spike" stall inception). The cause of the latter is not well understood; in axial machines it has been suggested that rotor blade-tip leakage flow plays an important role, but spikes have recently been observed in shrouded vaned diffusers of centrifugal compressors where these leakage flows are not present, suggesting an alternative mechanism may be at play.

This paper investigates the onset of instability in a shrouded vaned diffuser from a highly loaded turbocharger centrifugal compressor and discusses the mechanisms thought to be responsible for the development of short-wavelength stall precursors. The approach combines unsteady 3D RANS simulations of an isolated vaned diffuser with previously obtained experimental results. The unsteady flow field simulation begins at the impeller exit radius, where flow is specified by a spanwise profile of flow angle and stagnation properties, derived from single-passage stage calculations but with flow pitchwise mixed. Through comparison with performance data from previous experiments and unsteady full-wheel simulations, it is shown that the diffuser is accurately matched to the impeller and the relevant flow features are well captured.

Numerical forced response experiments are carried out to determine the diffuser dynamic behavior and point of instability onset. The unsteady simulations demonstrate the growth of short-wavelength precursors; the flow coefficient at which these occur, the rotation rate and circumferential extent agree with experimental measurements.

Although the computational setup and domain limitations do not allow simulation of the fully developed spike nor full-scale instability, the model is sufficient to capture the onset of instability and allows the postulation of the following necessary conditions: (i) flow separation at the diffuser vane leading edge near the shroud endwall; (ii) radially reversed flow allowing vorticity shed from the leading edge to convect back into the vaneless space; and (iii) recirculation and accumulation of low stagnation pressure fluid in the vaneless space, increasing diffuser inlet blockage and leading to instability. Similarity exists with axial machines, where blade-tip leakage sets up endwall flow in the circumferential direction leading to flow breakdown and the inception of rotating stall. Rather than the tip leakage flows, the cause for circumferential endwall flow in the vaned diffuser is the combination of high swirl and the highly non-uniform spanwise flow profile at the impeller exit.

INTRODUCTION

Modern internal combustion engines utilize high pressure ratio turbochargers combined with NO_x control strategies to improve efficiency and reduce emissions. In such an application, the centrifugal compressor design has to simultaneously achieve high efficiency, high pressure ratio, and a broad operating range. To meet these requirements, the trend has been towards highly loaded compressors, utilizing high speed impellers with backward-leaning blades for extended operating range and vaned diffusers for enhanced pressure recovery with compact geometry [1, 2].

The operating range of a compression system is limited by the onset of the well-known phenomena, rotating stall and surge [3]. A wide variety of stall and surge behavior in centrifugal compressors is reported in the literature, a consequence of the broad range of geometries in operation. For example, Hunziker and Gyarmathy [4] observed inducer stall, mild surge, deep surge, and diffuser rotating stall in a centrifugal compressor with different vaned diffusers; Frigne and Van den Braembussche [5] report diffuser rotating stall and impeller rotating stall (both abrupt and progressive) with a vaneless diffuser.

Prior to the onset of these fully developed instabilities, two distinct types of stall precursors have been identified: long

wavelength modal stall waves and short wavelength spikes [6]. While the presence of both types is well known in axial compressors and the occurrence of modal waves in centrifugal compressors is well documented (see, for example, [7-9]) the occurrence of spikes in centrifugal machines is a recent discovery [10].

The identification of stall pre-cursors has been a significant element of research into active control of compressors to extend operating range. For example, Skoch [11], Nelson et al. [12] and Spakovszky and Roduner [10] consider the use of air injection within the vaned diffusers of a centrifugal compressor upon early detection of stall or surge behavior, and report an extension in operating range (with some performance penalty).

Both analytical [13] and experimental work [4, 10, 11, 14] on centrifugal compressor stall inception indicates that for highly loaded stages with vaned diffusers the onset of instability typically occurs in the diffuser inlet region when operating at high speeds. This is the case both for modal and spike stall inception. The well-established principles of compression system modeling [13, 15, 16] are able to estimate the onset of instability where inception is via modal waves, with the time-evolution of flow field oscillations being linked to the background flow field. Spike stall inception, in contrast, cannot be captured in the same framework as it is a non-linear and three-dimensional flow breakdown. With the exception of [10], there exist no studies in the open literature examining the mechanism for short-wavelength "spike" stall inception in centrifugal compressors.

Two significant differences can be established in the pre-stall behavior of centrifugal compressors compared to axial machines: (a) multi-lobed backward traveling rotating stall waves form due to the relatively long convection times of vorticity waves shed from the impeller when interacting with downstream diffuser vanes [14] (in axial machines the blade-rows are much more closely coupled); and (b) spike-like disturbances stem from the stationary vaned diffuser without blade-tip gap leakage flows (in axial rotors, tip-clearance flows are conjectured to be connected with spike stall inception [6, 17]).

SCOPE OF PAPER

The main objective of this paper is to develop a set of necessary conditions for the onset of short wavelength instability in vaned diffusers. It is hypothesized that spanwise flow non-uniformity at diffuser inlet and the highly swirling flow in the vaneless space play critical roles in the formation of short wavelength "spike" stall precursors in vaned diffusers. Blade tip leakage flows, present in the rotor of axial machines when spikes are born, cannot be a necessary requirement in the formation of spikes in the shrouded vaned diffuser.

This paper describes numerical investigations of a highly loaded vaned diffuser from a pre-production turbocharger centrifugal compressor with a design pressure ratio of 5. The compressor has 9 main impeller blades, 9 splitter blades and 16 diffuser vanes. Experiments revealed that the diffuser experienced both modal waves and spikes at high speed, with a small bleed flow in the vaneless space altering the diffuser matching and changing the stall inception behavior [10]. This makes the design an appropriate candidate for further numerical investigation of the stall inception process.

At design corrected speed, the 3D RANS simulations indicate significant spanwise skew in impeller exit flow angle near stall; much greater than is present at 78% corrected design speed, as indicated in Figure 1. The flow is shown mixed out in the pitchwise direction via a control volume approach and both operating points relate to the last converged solution obtainable with a single passage model, utilizing a mixing plane at the rotor-stator interface.

The skew at 100% corrected design speed is caused by significant flow reversal near the shroud due to shroud endwall boundary layer growth (the convex shroud curve is more susceptible to boundary layer growth than is the concave hub curve) and tip gap effects through the impeller. A corresponding transfer of flow to the hub side results in increased radial velocity (reduced flow angle) between 0% and 30% span. In contrast, at 78% design speed the profile is more uniform from hub to shroud and shows no flow reversal. The implications are significant differences in the endwall flows and in the variation in incidence across the diffuser vane leading edge.

These differences present the opportunity to directly investigate the working hypothesis: the spanwise flow non-uniformity governs the type of stall inception.

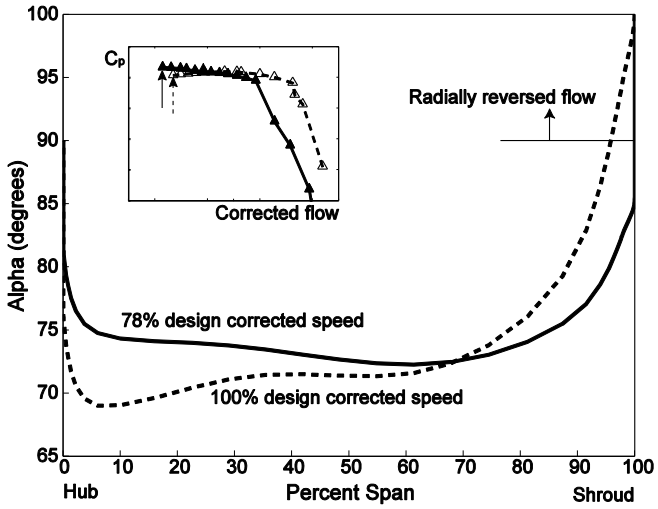

Figure 1: Comparison of flow angles near stall at different operating speeds. Inset shows stage speedlines from single passage, mixing plane CFD.

NOMENCLATURE

δz	Axial element
θ	Circumferential direction
ϕ	Flow coefficient, V_r/U
ρ	Density
C_p	Pressure coefficient
$\dot{m}$	Mass flow

n	Number of blades
p	Pressure
t	Time
T	Temperature
U	Impeller tip speed
V	Flow velocity
z	Spanwise dimension (axial in diffuser)

Subscripts

c	corrected (mass flow)
r	radial
m	mean
t	stagnation quantity
θ	circumferential
z	axial

Abbreviations

CFD	Computational Fluid Dynamics
PDPR	Peak Diffuser Pressure Rise
RANS	Reynolds Averaged Navier Stokes
SVLS	Semi-Vaneless Space
VLS	Vaneless Space

APPROACH

The work presented here forms part of a larger research effort on diffuser flow instability which combines experimental data with high fidelity unsteady 3D RANS simulations and reduced order modeling, where blades are replaced by a body force representation [18].

This paper considers the simulation of the diffuser flow in the commercially available RANS code Numeca FINE/Turbo, utilizing the single-equation Spalart-Allmaras turbulence model. The computational domain begins immediately downstream of the impeller tip, contains the vaneless space and the airfoil diffuser, and ends with a computational buffer zone to damp any possible reflections at the exit boundary. Neither upstream components (impeller) nor downstream components (volute) are included in this "isolated diffuser" model - its viability and limitations are topics of this paper.

The conceptual approach is summarized in Figure 2. The impeller outflow is modeled by carefully pitchwise averaging the non-uniform flow at the impeller exit plane taken from a single passage, steady RANS simulation with a mixing plane. The result is therefore a profile which varies from hub to shroud at the diffuser inlet, but where the flow direction and total conditions are uniform in the circumferential direction. The exit condition is chosen to be a uniform static pressure, adjusted to set the corrected flow at inlet to the diffuser.

Results from these simulations are compared with experimental data to determine their validity. Both quasi-steady performance data and fast response unsteady data describing the stall inception process are available from the experiments performed in [10]. In addition, unsteady full wheel simulations near the stall point are performed for validation of the isolated diffuser model. The comparison thus compares three models of the diffuser flow field to the experimental data: the isolated diffuser model; the unsteady full wheel model; and the single passage, steady, mixing plane model. It is shown that the standard mixing plane model suffers significant limitations when used in transonic centrifugal compressors, whereas the isolated diffuser simulations accurately capture the diffuser flow field.

To test for stability, a numerical "forced response" experiment is performed, whereby a perturbation is applied to the diffuser inlet flow, and the response of the flow is analyzed within a time-accurate simulation. A given operating point is deemed to be unstable if the unsteady response grows over time; conversely, if the solution returns to the same steady state as prior to the perturbation, the operating point is deemed to be stable.

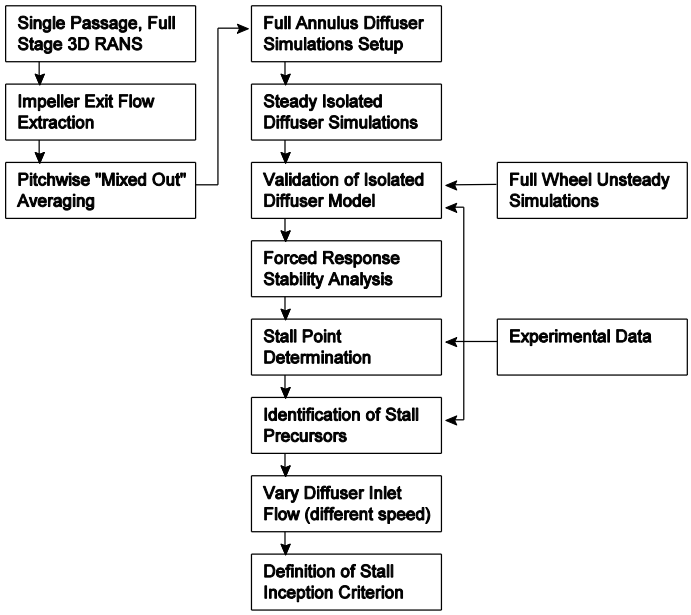

Figure 2: Conceptual approach.

The isolated diffuser simulations have several benefits. Most importantly, given the objectives of this research, it is possible to directly specify the spanwise flow non-uniformity in the vaneless space. This not only allows straightforward modeling of several speeds and operating conditions, but also enables parametric variation of the diffuser inlet flow profiles to distinguish the critical features of the flow.

Secondly, by pitchwise averaging the impeller outflow profile, the unsteady jet-wake flow at impeller outlet is reduced to a steady flow with pitchwise uniform stagnation properties and flow angle. This allows isolation of the effects of spanwise flow non-uniformity from the unsteady impeller-diffuser interaction, readily resolving small unsteady flow features (e.g. stall precursors) independently from the impeller jet-wake. Whether the diffuser can be studied in isolation from the impeller has been the subject of much research. It is now firmly established that the unsteadiness resulting from the jet-wake

impeller exit flow persists through the diffuser (see, for example, [19, 20]). However, it has been suggested, using both numeric analysis and careful experimentation, that the effects of unsteadiness on the diffuser flow are small relative to the effects of the time-mean spanwise flow non-uniformity in the impeller exit flow [21-23]. This is also the foundation for the use of the "mixing plane" in steady CFD simulations.

Further assessment is performed through detailed comparison of the isolated diffuser flow field with the time-mean solution from an unsteady, full wheel simulation. Good agreement was found and further detail is provided in [24]. The full wheel simulations suggest that the reversed flow region at the shroud is underestimated in the mixing plane simulations. This is in line with the findings of Shum et al. [22], who observed that the unsteady upstream influence of the diffuser vanes on the impeller [25] had a greater effect than did the unsteady impeller flow on the diffuser.

It is important to note, however, that impeller-diffuser interaction provides a mechanism for modal waves to develop [14] and hence it is not expected that the isolated diffuser model will be capable of capturing this route to instability. For modeling modal waves, the research currently relies on the body force approach described in [18].

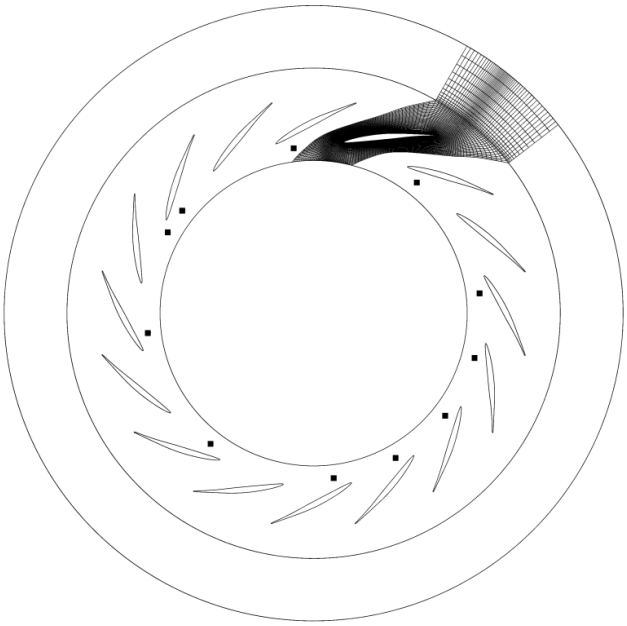

Figure 3: Computational domain and vaneless space fast-response pressure sensor array location. For clarity, mesh is shown only for one passage.

Lastly, modeling just the diffuser allows a full annulus model (desirable for accurately capturing the development of stall precursors and their rotation rate) to be performed at a reasonable computational cost, while maintaining a computational mesh capable of capturing the fine features of the flow. The mesh comprised approximately 4 million mesh nodes.

MODEL FORMULATION AND CHALLENGES

Given the model domain, there are two boundary conditions that require careful definition to accurately model the diffuser flow: inlet and outlet. The definition of the inlet flow properties calls for a modified mixing plane approach to obtain a pitchwise uniform diffuser inlet flow. Care must be taken at the exit boundary to accurately represent the exit condition and avoid non-physical reflections. The real compressor utilizes a downstream volute but this is often neglected in computational models of centrifugal compressors due to the complexity involved in its modeling (for example, it removes the axi-symmetry upon which single passage simulations rely).

To obtain the pitchwise average diffuser inlet flow profile, a control volume approach is taken to fully mix out the flow in the pitchwise direction. The impeller exit flow is taken from single passage, steady simulations. For improved accuracy but increased computational cost, it would be possible to use full wheel unsteady simulations as an alternative to generate the isolated diffuser inlet conditions.

To perform the control volume analysis, the span is divided into elements and the flow at each spanwise location is mixed out conserving mass, momentum and energy, as per equations (1) - (5)[1]. The left hand side represents the pitchwise non-uniform flow at each spanwise location z ("upstream" side of control volume) and the right-hand side represents the mixed out average state for defining the boundary conditions ("downstream").

Conservation of mass:

$$\int_0^{2\pi/n} \rho V_r \, \delta z \, r \, d\theta = \bar{\rho}\overline{V_r}(2\pi r/n) \, \delta z = \dot{m} \tag{1}$$

Conservation of radial, tangential and axial momentum:

$$\int_0^{2\pi/n} (p + \rho V_r^2) \, \delta z \, r \, d\theta = (\bar{p} + \bar{\rho}\overline{V_r}^2)(2\pi r/n) \, \delta z \tag{2}$$

$$\int_0^{2\pi/n} \rho V_r V_\theta \, \delta z \, r \, d\theta = \dot{m} \, \overline{V_\theta} \tag{3}$$

$$\int_0^{2\pi/n} \rho V_r V_z \, \delta z \, r \, d\theta = \dot{m} \, \overline{V_z} \tag{4}$$

Conservation of energy:

$$\int_0^{2\pi/n} \rho V_r c_p T_t \, \delta z \, r \, d\theta = \dot{m} c_p \overline{T_t} \tag{5}$$

At the downstream side of the control volume, the flow angle and the stagnation conditions can thus be calculated. The control volume is collapsed to a plane at the impeller exit

[1] This definition differs from the "momentum averaged" flow angle used by Filipenco et al. [26] where the inlet flow angle was averaged over span to characterize experimentally measured diffuser inlet conditions by one parameter. Here, mixed out averaging provides a physically meaningful method to describe an equivalent, spanwise distribution of pitchwise mixed flow at inlet to the diffuser.

radius, essentially becoming a "mixing plane", supplying the isolated diffuser with inlet boundary conditions. Note that only stagnation quantities and the velocity direction are held constant in the circumferential direction within the definition of the inlet conditions of the isolated diffuser simulations. Static quantities and the velocity magnitude are allowed to vary. The pitchwise average values calculated in the control volume (e.g. $\bar{p}$ or $\overline{V_r}$) are only present as an interim step in the calculations.

The steady mixing plane calculations diverged at corrected flows higher than the experimentally measured stall point. It was therefore necessary to extrapolate the inlet conditions to allow isolated diffuser simulations at lower flow. The extrapolation was based on observed trends for operating points near to stall: diffuser inlet flow angle and total temperature varied linearly with mass flow while a quadratic dependence was found for total pressure variations over the small mass flow range of interest. Extrapolation was performed only to 10% below the corrected flow of the last operating point in the single passage simulations.

Finally, to complete the model setup, the exit boundary conditions need to be considered. The volute is known to impose a strong circumferential non-uniformity throughout the compressor [1], and provides a downstream volume that can allow surge. It is hypothesized that the mechanism for stall inception can be captured without the volute, although the fully developed instability towards which the compressor tends and the precise corrected flow at which the diffuser flow enters an unstable regime may be altered. Thus, a uniform exit boundary condition is selected here, chosen so as to achieve the diffuser inlet corrected flow of the single passage simulation. Further investigation on the role of the volute on stability is currently in progress.

The exit boundary needs to be carefully implemented in unsteady simulations to prevent wave reflections [27]. A mass flow boundary condition is preferred close to stall as small changes in the diffuser pressure ratio result in large changes in the diffuser inlet corrected flow. Mass flow boundary conditions are available within FINE/Turbo but were determined to be unsuitable for purposes of the stability assessment[2]. The alternative is to apply a static pressure. A uniform pressure boundary typically causes reflections by acting as a pressure node. A "buffer zone" with expanding cells is necessary to numerically damp pressure waves traveling out of the diffuser passage and possibly reflecting back from the exit boundary. It is noted that the volute inlet presents a change in impedance to waves exiting the diffuser, which could allow wave reflections. This is one aspect of the volute flow that is under further research.

In summary, the isolated diffuser model is defined from the impeller trailing edge with the impeller exit flow modeled via pitchwise mixed-out stagnation conditions and flow angles, and extends through a buffer zone to a uniform static pressure exit condition.

MODEL VALIDATION WITH STEADY-STATE EXPERIMENTAL DATA AND UNSTEADY CFD

The isolated diffuser was validated through comparison with experimental data from [10] and unsteady, full wheel simulations run near stall specifically for validation purposes.

The experimental data allows dissection of the steady-state diffuser performance through the subcomponent pressure rise characteristics. The qualification of a "good" model for the purposes of assessing stability is primarily the agreement in the slopes of the characteristic curves [4]. In particular, the semi-vaneless space is identified as the critical subcomponent by several authors (e.g. [4, 10]), therefore good agreement in this subcomponent is important. The flow near stall is particularly sensitive to blockage, and the combination of unsteady effects and the limitations in turbulence modeling make it challenging to achieve precise agreement in the component static pressure rise [28].

Given the above criteria, Figures 4, 5 and 6 show good agreement between the isolated diffuser model and the experiments. Firstly comparing the isolated diffuser model to the experiments, Figure 4 shows that, at 100% corrected design speed, the slope of the diffuser characteristic changes from negative to positive at low corrected flows. The corrected flow at which this occurs is well captured in the isolated diffuser model.

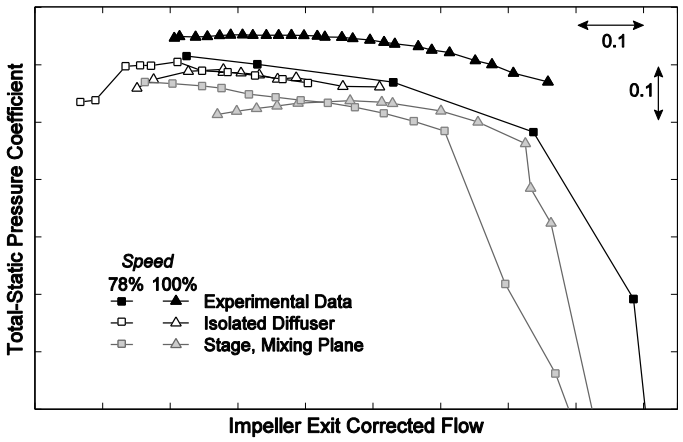

Figure 4: Diffuser static pressure rise coefficients at 78% and 100% design corrected speeds.

In contrast, at 78% corrected design speed, the experiments show the diffuser total-to-static pressure coefficient continues to increase until stall is reached. In the isolated diffuser simulations, the characteristic shows a drop in pressure rise at low corrected flows. This is the consequence of a hub corner separation, which grows dramatically at such low corrected mass flows. It is hypothesized that in the computation, the

[2] To allow convergence to a user-defined mass flow, information must be artificially inserted onto the exit boundary. This creates pressure waves that propagate back into the diffuser domain which must be avoided in stability analyses.

diffuser flow becomes statically unstable[3] at this operating point and moves to an alternative operating regime with severe separation in the diffuser passage. It is further hypothesized, as discussed below, that the compressor would actually reach dynamic instability before this occurs[4], as indicated in the experimental data. The computations show that the hub corner separation extends from the passage into the semi-vaneless space, as indicated clearly by the drop in pressure rise achieved in this subcomponent in Figure 6.

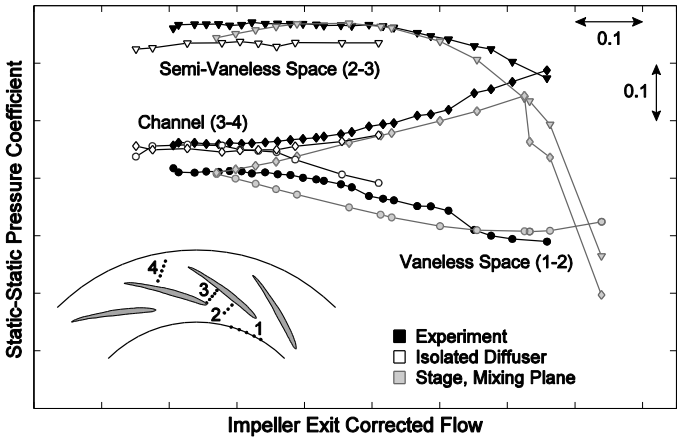

Figure 5: Subcomponent characteristics for 100% design corrected speed.

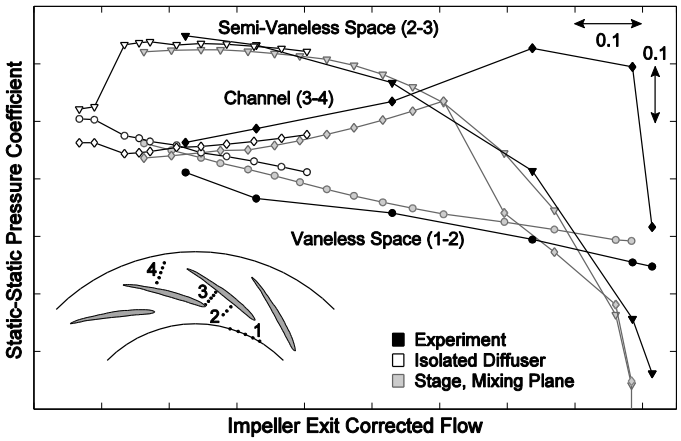

Figure 6: Subcomponent characteristics for 78% design corrected speed.

The vaneless space characteristic is negatively sloped across the operating range in the 78% speed case, stabilizing the diffuser flow, but at 100% speed levels off near to stall. This indicates that both the vaneless and semi-vaneless space are important to the stability of the compressor at 100% speed, while at 78% speed it is the semi-vaneless space that governs the point of instability. Note that the diffuser channel is unstable (positive slope of pressure rise characteristic) over almost the entire flow range for both speeds. This is because for lower mass flows the blockage near the throat grows as a consequence of the increasing adverse pressure gradient in the diffuser inlet region; in turn, the increased blockage results in a drop in pressure rise in the channel.

Camp and Day [6] stated that, for axial machines, spike stall inception can be expected if the critical vane incidence is exceeded before the peak in the total-to-static pressure rise characteristic. Neither the isolated diffuser nor the single passage steady simulations can capture modal stall inception, and therefore it is not possible to fully validate this criterion. It is observed that the 100% speed case, susceptible to spike stall inception, remains dynamically stable in the isolated diffuser model with a slightly positively sloped characteristic.

Spakovszky and Roduner [10] refined Camp and Day's criterion for a centrifugal compressor with a vaned diffuser, suggesting if the peak of the semi-vaneless space characteristic occurred prior to the peak of the overall diffuser characteristic, stall would be initiated by modal waves. The 78% speed case, shown later in the paper to be dynamically stable to spikes but unstable to modes, indicates that this criterion is met in this diffuser.

Comparing the isolated diffuser model to the single passage model employing the standard mixing plane, it is observed that good agreement is obtained at 78% design speed. However, at 100% design speed, the two models provide significantly different results, particularly in the slopes of the characteristics. This is examined through a comparison of the flow field, discussed next.

The diffuser flow field at 100% design speed is examined in Figure 7 through plotting the Mach number at midspan. The unsteady full wheel simulation is time-averaged and compared to the isolated diffuser and the single passage, stage simulation. The isolated diffuser simulation shows good agreement with the time-averaged result from the unsteady simulation, validating the pitchwise mixed out inlet conditions defined above. Further analysis (not presented here, see [24] for details) shows that the diffuser vane loading is also accurately captured in the isolated diffuser simulation, and that the effects of unsteady loading changes are negligible compared to the time-mean loading, validating the earlier hypothesis. In summary, the isolated diffuser model and the pitchwise mixed inlet flow conditions as defined above are in good agreement with the full-wheel unsteady CFD and experimental results.

The flow field in the steady, mixing plane simulation shown in Figure 7 illustrates the deficits of the standard mixing plane approach, supporting the observations made by other researchers [29, 30]. A much larger pressure side separation is observed in the single passage stage calculations due to misrepresented diffuser inflow conditions, governed by incomplete pitchwise mixing at the mixing plane. It is conjectured that this is exacerbated in centrifugal compressors with vaned diffusers by the strong upstream influence of the diffuser vane, the jet-wake structure from the impeller and

[3] Pure divergence from initial state (equivalent to negative stiffness).

[4] Static stability is necessary but not sufficient: dynamic instability (negative damping) leads to exponentially growing oscillations and is often reached first [3].

possibly local flow reversal (see [24] for further detail). At transonic operating points the flow field is particularly sensitive to the corrected flow and strict conservation across the mixing plane is not guaranteed in the standard model. At lower speeds, the agreement with the mixing plane solution is improved.

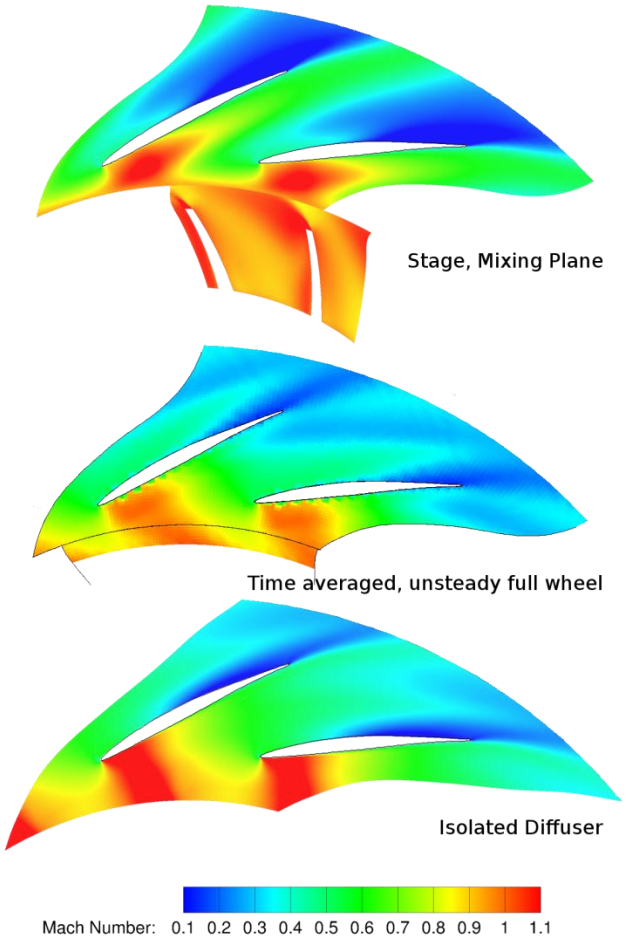

Figure 7: Diffuser flow fields at midspan at 100% design speed, near stall.

STABILITY ASSESSMENT AND MECHANISM FOR SHORT-WAVELENGTH STALL INCEPTION

A short duration forcing in total pressure is introduced at the inlet domain to determine the dynamic response of the vaned diffuser flow field. The forcing disturbance is an increase in total pressure of 25% of the diffuser inlet dynamic head, applied across 20% of the span from the shroud and 10° of the circumference for ¼ rotor revolution[5]. The short time and length scales allow excitation of various frequencies and spatial wavelengths. If the diffuser flow returns to the same equilibrium state as prior to the perturbation, the flow field is deemed stable.

[5] The form, location and timescale of the perturbation was varied in parametric studies, and it was determined the final response was largely insensitive when applied on the shroud side [24].

The effect of the different spanwise flow non-uniformity is examined through comparison of the forced response for two design corrected speeds. These have significantly different impeller exit flow profiles as discussed earlier in Figure 1.

100% design corrected speed

As the operating point of the diffuser moves toward stall, the following flow features are observed:

(i) as the flow coefficient $\phi = V_r/U$ at impeller exit reduces with the reduction in mass flow, the slip remains about constant, such that the diffuser inlet swirl angle increases; (ii) blockage at the shroud endwall increases at impeller exit, with reversed radial flow developing near the shroud as the low momentum flow perceives the strong radial pressure gradient caused by the high bulk swirl; (iii) the spanwise extent of the reversed radial flow increases from the shroud side as inlet

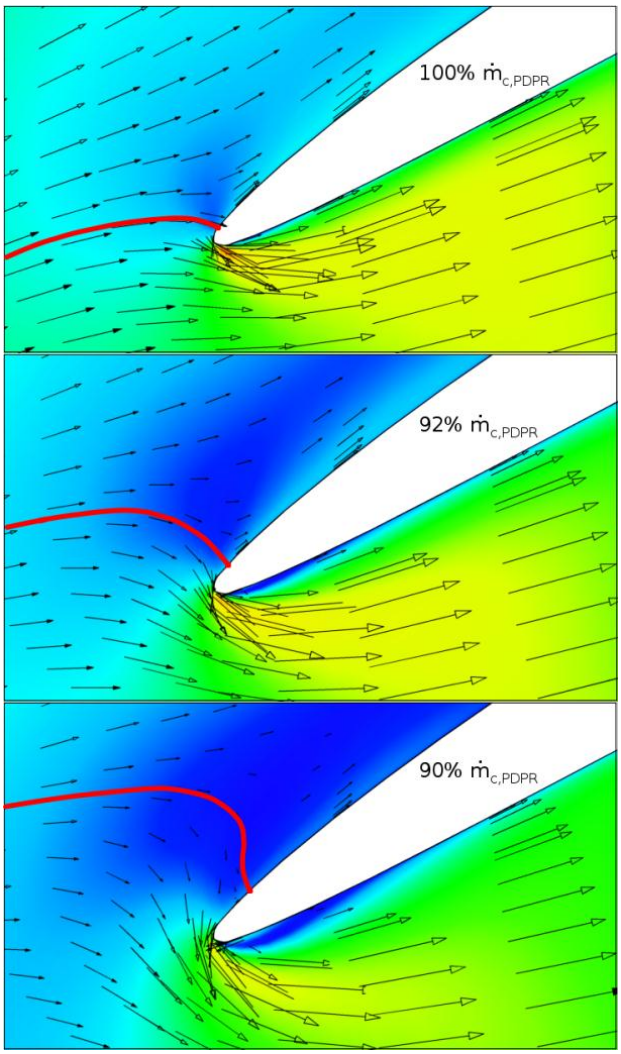

Figure 8: Mach number contours and velocity vectors at 90% span and near vane leading edge for operating points close to stall at 100% speed. The stagnation streamline is indicated in red.

corrected flow is further reduced; (iv) a region of recirculating flow develops in the vaneless space and close to the shroud, fluid can circulate around the entire circumference; (v) when the incidence on the diffuser vanes close to the shroud exceeds a critical value a separation bubble forms on the suction side of the leading edge. Figure 9 shows the leading edge separation bubble developing as the operating point of the diffuser moves towards stall: the low Mach region (blue) indicates the extent of the bubble and the streamlines show the movement of the stagnation point further downstream on the vane as the corrected flow is reduced.

These features are important to the development of unstable flow in the diffuser following the perturbation as discussed next.

The introduction of a local disturbance, provided here by the perturbation in total pressure at the inlet boundary, alters the local corrected flow and thus the diffuser vane loading. Some fraction of the bound circulation is shed at the leading edge, where there exists a flow separation. The reversed radial flow present near the shroud allows the vortical and low total pressure fluid shed from the vane to convect back into the vaneless space.

At the diffuser inlet, the flow angle is nearly tangential; at the lowest flow operating point simulated it exceeds 80° from radial for 12% of the span, from the shroud side. This allows the disturbance to convect around and impact the neighboring vane. Again, this vane sheds a proportion of its bound circulation, which convects back into the vaneless space and combines with that from the previous vane.

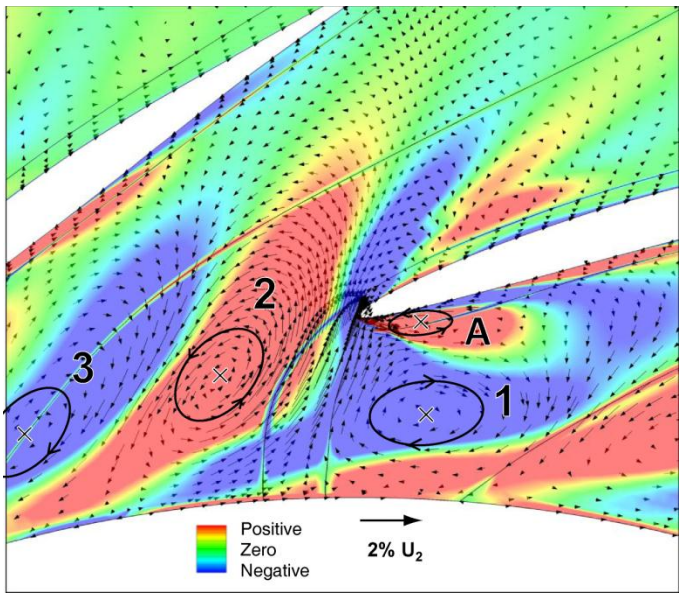

Figure 9: Time snapshot of counter-rotating vortical structures 1, 2 and 3 convecting in vaneless space at 90% span. Vorticity shed from leading edge (A) merges with passing vortical structure 2 at a later time.

Over time, a series of counter-rotating vortical structures form in the vaneless space and convect around the vaneless space as shown in Figure 9. This low stagnation pressure fluid is trapped in the recirculating flow region near the shroud depicted in Figure 10, which shows streaklines for particles released in the vaneless and semi-vaneless space at the span indicated in the left column. Two operating points are shown: at peak diffuser pressure rise (PDPR) and an operating point with 10% lower flow coefficient. The latter was unstable following a perturbation to the inlet flow.

The vortical structures are marked by the numbers in Figure 9, where the perturbation velocity vectors, defined by:

$$\overrightarrow{V'} = \vec{V}(t) - \vec{V}_m \tag{6}$$

are plotted. Also shown is the change in axial vorticity from the steady state solution. These are two alternative methods for visualization of the shed vorticity and the counter-rotating vortical structures.

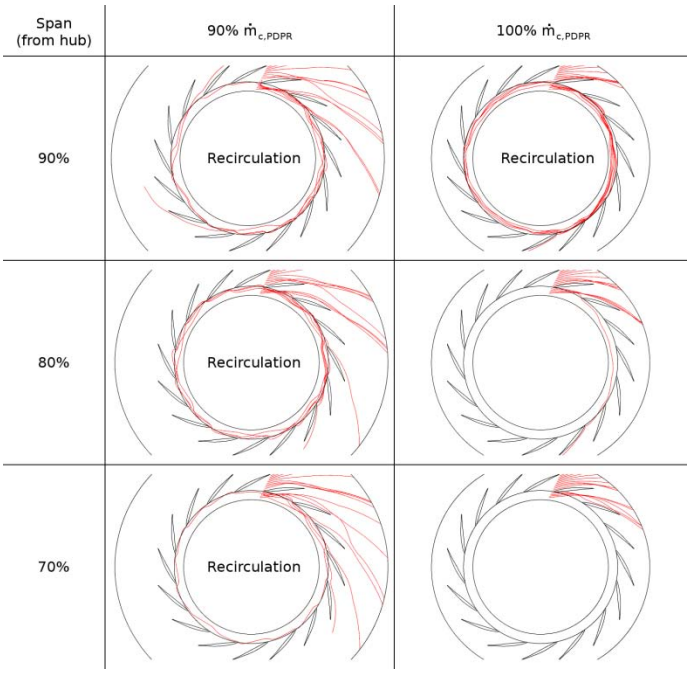

Figure 10: Flow near shroud recirculates in the vaneless space over a larger spanwise extent as diffuser inlet corrected flow is reduced; combined with separation from the vane leading edge, conditions on left allow short wavelength stall inception.

Figure 11 shows data from an array of static pressure taps around the vaneless space (as shown in Figure 3). The pressure signals are non-dimensionalized by the inlet dynamic head, and are spaced according to their circumferential position. As the vortical structures pass a vaneless space pressure tap, the sensor records the low pressure at the center of each vortical structure and the higher pressure at the edges, resulting in the observed

high-frequency oscillations[6]. The disturbance is thus represented as a region of high-frequency pressure oscillations at each pressure tap location. The disturbance can be seen to cover an increasing number of diffuser passages. Figure 11 also allows verification of the transport velocity of the vortical structures; this is approximately 30% of the rotor speed, corresponding to the tangential velocity of the shroud endwall fluid.

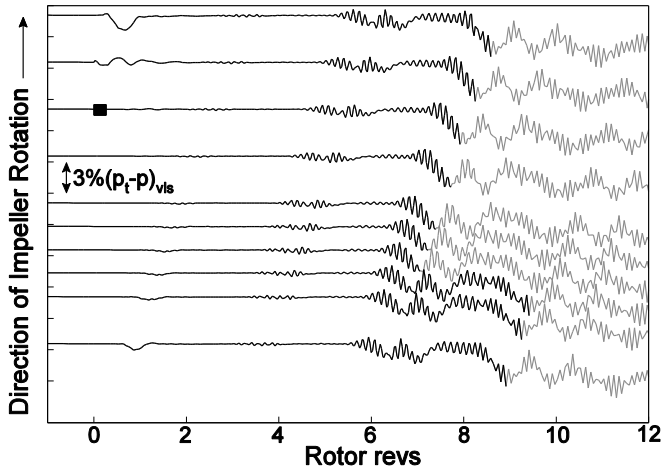

Figure 11: Computed static pressure traces in the vaneless space at 100% design corrected speed for the operating point at 90% $\dot{m}_{c,PDPR}$. The small black box represents duration and spatial extent of the initial forcing function.

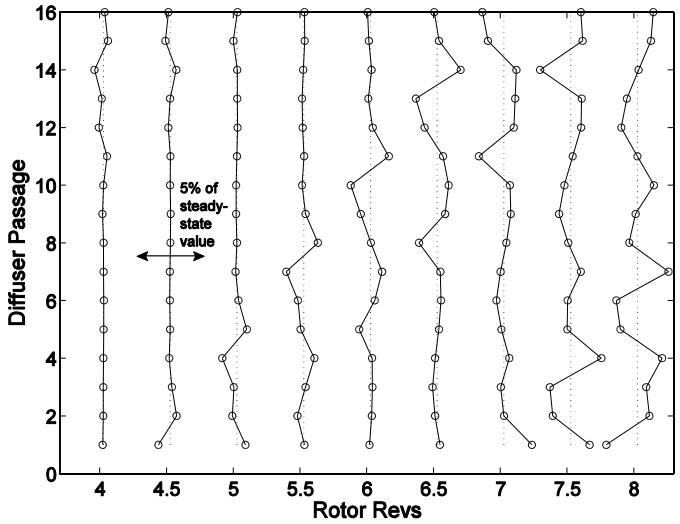

Figure 12: Variation in diffuser passage inlet corrected flow as low stagnation pressure vortical structures pass by.

The disturbance grows in the isolated diffuser simulations until a large pressure drop occurs at each diffuser vane from which the flow can no longer recover back to the initial state. Due to the domain limitations of the isolated diffuser calculation a fully developed stall cell with significant reductions in average mass flow and diffuser pressure rise cannot be established. Furthermore, the geometrical extent of the vortical structures present in the vaneless space is constrained by the inlet boundary condition applied: the pitchwise uniform inlet flow angle prescribed prevents further growth. In the real device the growth of the vortical structures could continue back into the impeller passage (noting that the radial flow is reversed near the shroud endwall where these feature develop). The transition from black to gray in Figure 11 is thus suggested as a limit where the isolated diffuser model no longer accurately captures the developing instability.

The development of vortical structures in the vaneless space alters the diffuser inlet blockage and has a significant effect on the loading of the vaneless and semi-vaneless space. To assess blockage, Figure 12 illustrates the variation in corrected flow for the 16 diffuser passages (each circle corresponds to one passage) at the plane of the diffuser vane leading edge as a function of time following the perturbation. The disturbance initially affects about four passages but extends rapidly to cover roughly eight passages at six rotor revolutions after application of the total pressure forcing at the diffuser inlet. By eight rotor revolutions, the corrected flow varies by as much as ±2.5% for a given passage as the low stagnation pressure vortical structures convect past. In addition, the axial extent of the vortical structures is observed to increase over time from 20% to 30% of the span from the shroud (not shown).

The convection of the disturbance in the vaneless space sets up a feedback mechanism: the traveling disturbance causes vane loading variations, and the shed vorticity convects backwards into the vaneless space to add further to the disturbance. This feedback mechanism leads to increasing blockage in the vaneless and semi-vaneless space. It is conjectured that this eventually leads to the formation of an embryonic stall cell, causing the pressure "spike" seen in experiments of the order of the inlet dynamic pressure.

A discussion of the similarities and differences between these findings and the observations from experiments in [10] follows in the next section.

78% design corrected speed

The spanwise flow profile as the compressor is throttled towards stall along the 78% corrected speedline is markedly different from the 100% speedline case, as shown in Figure 1. Particularly, the flow angle at the shroud is significantly lower (more radial). The diffuser no longer experiences radial flow reversal near the shroud or separation from the shroud side vane leading edge, as shown in Figure 13. The most noticeable behavior is the growth of a large hub corner separation in the diffuser channel, which occupies an increasing proportion of the chord until a sudden drop off in performance can be detected in the semi-vaneless space, as indicated in the characteristics in Figure 6. In contrast to the 100% speedline

[6] The vortical structures have been identified through animation of the unsteady flow field; the oscillation frequency agrees with the convective flow velocity and the spacing of the vortical structures.

(Figure 5), the vaneless space maintains a positive gradient consistent with stabilizing behavior [4].

No dynamically unstable behavior could be triggered in the isolated diffuser simulation at 78% corrected design speed: the flow field returns to the same equilibrium state when perturbed either near hub or near shroud and for operating points on both sides of the step in the characteristic. Figure 14 shows the response from a perturbation at the operating point immediately to the right of the drop in the static pressure rise characteristic curve. It is evident that the diffuser flow field is dynamically stable at this point, since the flow field returns to the initial steady state following the perturbation.

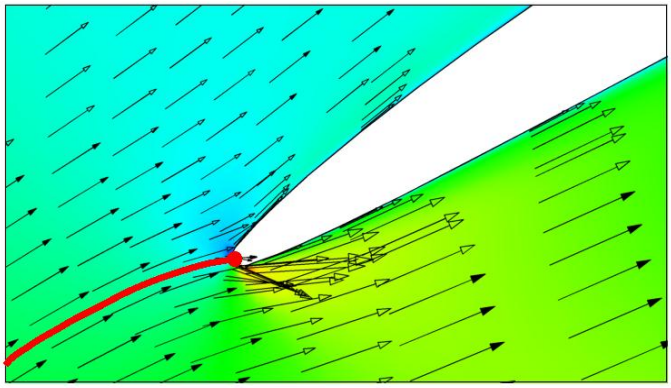

Figure 13: Mach number contours and velocity vectors at 90% span and near vane leading edge for an operating point close to stall at 78% speed. The stagnation streamline is indicated in red.

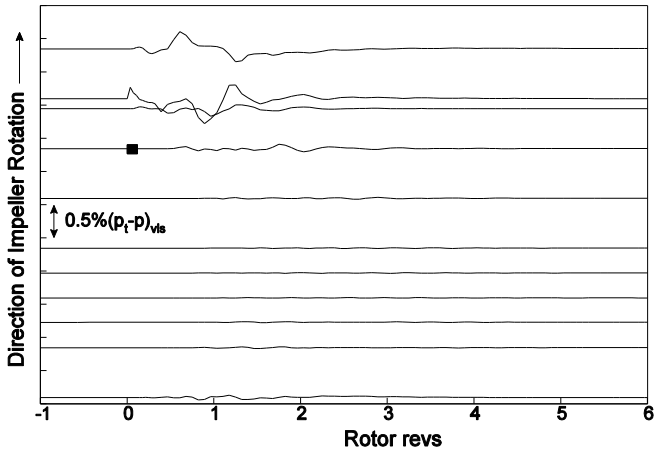

Figure 14: Computed static pressure traces in vaneless space at 78% design corrected speed for the PDPR operating point. The small black box represents duration and spatial extent of the initial forcing function.

The result of these forced response tests suggests that the lower speed flow is not susceptible to short-wavelength stall inception, unlike the 100% speedline. The vaneless space is strongly stabilizing: effective diffusion occurs throughout the vaneless space, even as flow coefficients into the diffuser are reduced. Without flow reversal in the vaneless space near the shroud, and with significant hub separation further along the diffuser vane chord, the dynamic behavior of the diffuser changes. These features are a consequence of the diffuser inlet conditions, particularly the spanwise flow profile applied: with a more uniform flow profile, the shroud endwall flow is able to withstand the radial pressure gradient imposed by the swirl and the effects that are hypothesized to lead to short-wavelength stall inception are not triggered.

COMPARISON WITH EXPERIMENTS

100% design corrected speed

The findings from the isolated diffuser RANS simulations can be compared directly against fast-response measurements taken previously on the same compressor geometry [10]. Plots of pressure variations from the time-mean for a series of pressure taps distributed at the same locations around the vaneless space are shown in Figure 15. The rotation rate shows good agreement between experiment and CFD.

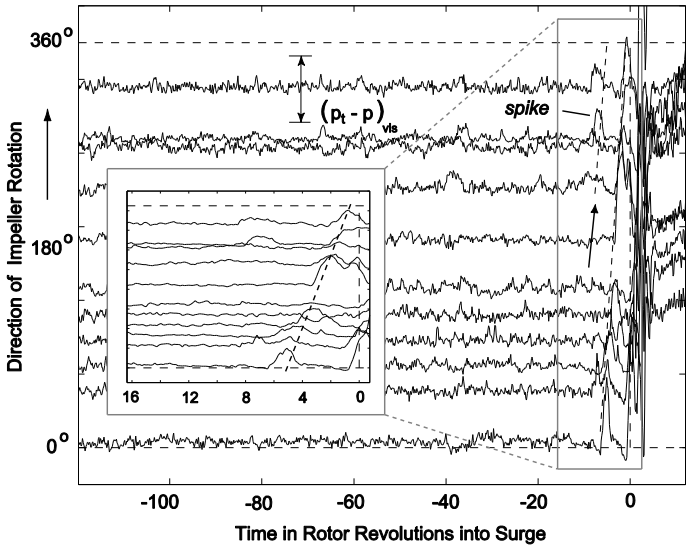

Figure 15: Experimentally measured static pressure traces in the vaneless space at 100% design corrected speed, adopted from [10]. The short-wavelength precursor is identified via the dotted line.

As discussed above, the high frequency component present in the CFD result arises from the convection of vortical structures past pressure taps, with low pressure in the core region of each structure. These oscillations cannot be seen in the experimental data probably for the following reasons: (i) the sampling frequency used in the experiments was 3 kHz which is insufficient to capture these oscillations (in the CFD data they are plotted at an equivalent of 8 kHz sampling frequency); and (ii) the oscillations may simply be lost in the noise of the experimental data with the amplitude of the pressure

oscillations too low to capture, until they cause large-scale flow breakdown in the diffuser.

The pitchwise extent of the disturbance (indicated between 4 and 6 rotor revolutions in the CFD results in Figure 11 and -6 to -4 rotor in the experimental data in Figure 15) show reasonable agreement. The disturbance covers approximately 8 passages in both the isolated diffuser simulations and the experiments.

78% design corrected speed

Fast response data for the 78% corrected design speed is not available from the experiments in [10]. However, body force based simulations from related work documented in [18] suggest the diffuser stall inception process is modal at the lower speed. This behavior cannot be captured in the isolated diffuser model.

Figure 16, adopted from [18], depicts unsteady pressure traces computed using a 3D unsteady full wheel Euler calculation with body forces for the same compressor stage at 75% corrected speed. Backward traveling waves are observed indicating modal stall inception.

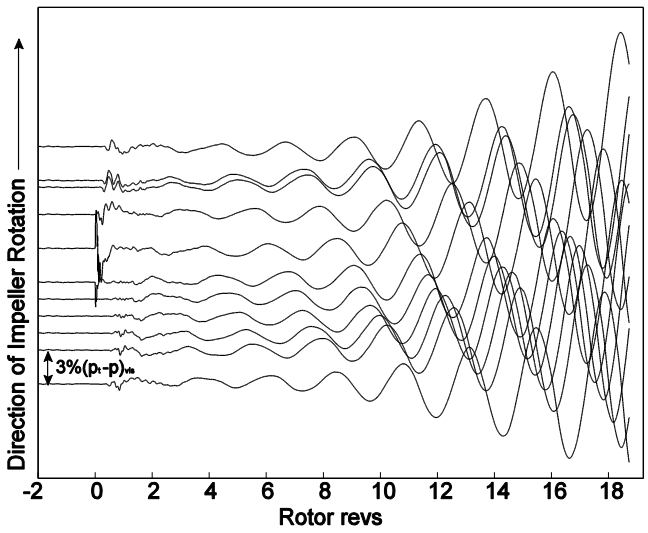

Figure 16: Computed static pressure traces in the vaneless space using full wheel body force simulation at 75% design speed, adapted from [18]. Backward traveling modal waves are observed prior to stall.

SUGGESTED CRITERIA FOR SHORT-WAVELENGTH STALL INCEPTION

The observed behaviors at different speeds with this compressor suggest the following features, summarized in Figure 17, are necessary for the formation of short-wavelength stall precursors:

1. Separation at the diffuser leading edge caused by high incidence near the shroud endwall, allowing vorticity to be shed from the diffuser vane leading edge with changes in diffuser vane loading;
2. Locally reversed radial flow in the vaneless and semi-vaneless space allowing vorticity shed from the leading edge to convect back to the vaneless space;
3. Flow in the vaneless space that recirculates around the circumference, allowing vortical structures to form and to grow through the addition of vorticity shed from the diffuser vane leading edge; and
4. A feedback mechanism whereby the convection of the vortical structures within the developing stall precursor triggers a variation of incidence on the downstream blade, such that further vorticity/low total pressure fluid sheds from that vane and causes growth of the precursor.

These features are a consequence of the reversed radial flow near the shroud, itself caused by the radial momentum deficit in the shroud endwall flow at exit from the impeller. It is suggested that careful control of the impeller exit flow profile could allow alteration of the dynamic behavior such that the onset of instability could be delayed.

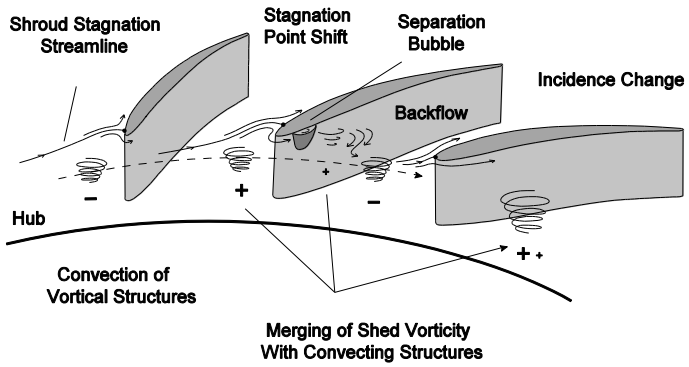

Figure 17: Suggested mechanism for short-wavelength stall inception in vaned diffusers.

THOUGHTS ON SIMILARITIES WITH AXIAL COMPRESSORS

In axial compressors, spike stall inception has been linked with blade tip spillage flow, but the diffuser of the centrifugal compressor described above is shrouded with no tip leakage. It is of interest to determine whether there are similarities between the two observed stall phenomena.

Vo et al. [31] set out two criteria for spike stall inception in an axial machine, based on the results of computational work: (a) the interface between tip leakage flow and the oncoming flow becomes parallel with the leading edge plane; and (b) backflow occurs from the trailing edge plane of the blade row. There exists some experimental evidence for these hypotheses (e.g. [32]). The first of Vo et al.'s criteria has similarity to the effects observed above; the recirculation of flow in the vaneless space results in oncoming flow near the endwall being parallel to the diffuser vane leading edge plane. Rather than tip leakage flows causing this circumferential flow, as observed in axial

compressors, the cause in centrifugal compressors is the high swirl at diffuser inlet and the momentum deficit at the shroud.

Inoue et al. [33-35] examined short- and long-wavelength stall inception in an axial compressor stage. They hypothesized that a separation vortex forms on the suction side of a blade near the casing in an axial machine, causing a low pressure region upstream of the blade which is observed in experiments. They observe that the separation may be at the leading edge in the early stages of the stall precursor development. The work here suggests the development of vortical structures near the casing/shroud endwall may be a common factor in spike stall in both axial compressors and in the vaned diffusers of centrifugal compressors.

Finally, it is observed that the short-wavelength stall inception observed in the simulations described above and in the experiments of [10] differs from that observed in axial compressors in the pitchwise extent of the "spike". It is hypothesized that this difference may lie in the difference in the inter-blade-row spacing and solidity of the two machines. The centrifugal compressor allows the growth of a significantly larger flow disturbance upstream of the diffuser vanes; in the axial compressor, unsteady flow features are much more geometrically constrained.

CONCLUSIONS

An isolated diffuser model has been developed to study the onset of stall inception in a high speed centrifugal compressor, and validated through comparison to previously collected experimental data. The dependence of the route to instability (short wavelength "spikes" or long wavelength "modes") on the impeller exit flow profile is examined through comparison of two different speedlines, which were observed to provide significantly different hub-to-shroud impeller exit flow profiles. The following conclusions are made:

- An isolated diffuser model which models the impeller outflow spanwise flow profile in a physically representative manner is capable of capturing short wavelength stall inception in the vaned diffuser of a centrifugal compressor.
- The standard mixing plane used to model the rotor stator interface in RANS simulations is shown to be deficient for transonic centrifugal compressors with vaned diffusers due to the sensitivity to corrected flow, the strong upstream influence of the diffuser vane and the strong circumferential flow non-uniformity imposed in the vaneless space by the impeller jet-wake flow.
- The isolated diffuser model allows the hypothesis of a mechanism for short wavelength stall inception in centrifugal compressors with vaned diffusers: spanwise flow non-uniformity can allow flow angles approaching and exceeding 90° in the vaneless space, causing separation on the shroud side of the vane leading edge and radial flow reversal near the shroud throughout the vaneless and semi-vaneless space. Upon the disturbance of the diffuser vane loading and shedding of diffuser vane bound circulation, vorticity shed from the leading edge can convect back into the vaneless space. Vortical structures develop which increase diffuser inlet blockage and destabilize the diffuser. This was observed at 100% design speed; the precursor that develops in the simulations is shown to be similar to the experimentally measured short-wavelength stall precursor.
- Where the spanwise flow profile at impeller exit is more uniform, without large changes near the endwalls, this mechanism is not triggered, as shown in the 78% design speed case. Here the compressor stalls via modal waves instead, which cannot be modeled in the isolated diffuser. The pressure rise characteristic for the vaneless space is negatively sloped and thus stabilizing throughout the operating range at 78% design speed, such that the diffuser inlet region is no longer the critical subcomponent.
- In axial compressors, the endwall flow has been identified as critical in the literature, but the focus has been on the development of tip leakage flows allowing tangential endwall flow parallel to the blade row leading edge. In centrifugal machines, tangential endwall flows are generated due to high swirl in the bulk flow and a radial momentum deficit near the shroud endwall.

Further experiments are planned to examine the proposed mechanism through high speed data collection in the endwall regions. The experiments will further examine the effect of spanwise flow non-uniformity and will consider a variety of different diffuser configurations.

In addition, experiments and further CFD including the volute are important to categorize the role of the volute on the stall inception process.

ACKNOWLEDGMENTS

The authors would like to thank the other members involved in centrifugal compressor stability work at MIT, past and present, upon which this work builds. Firstly, Mr. B. Kuschel is thanked for his thorough analysis of the performance of the compressor at lower speed. Mr. B. Benneke developed a body-force model for this compressor, and Mr. R.A. Hill initially worked on the isolated diffuser concept. Prof. N. Cumpsty is also acknowledged for his comments and suggestions throughout the project. This research was funded by ABB Turbo Systems Ltd. which is gratefully acknowledged.

REFERENCES

[1] Cumpsty, N., 2004, "Compressor Aerodynamics", Reprint Edition, Kreiger Publishing Company, Malabar, Florida.

[2] Japikse, D., 1996, "Centrifugal Compressor Design and Performance", Concepts ETI, Inc.

[3] Greitzer, E., 1981, "The Stability of Pumping Systems - The 19810 Freeman Scholar Lecture," J. Fluids Engineering, 99, pp 193-242.

[4] Hunziker, R., and Gyarmathy, G.., 1994, "The Operational Stability of a Centrifugal Compressor and Its Dependence on the Characteristics of the Subcomponents," ASME J. Turbomach., 116, pp. 250-259.

[5] Frigne, P., and Van Den Braembussche, R., 1984, "Distinction Between Different Types of Impeller and

Diffuser Rotating Stall in a Centrifugal Compressor with Vaneless Diffuser," ASME J. Eng. for Gas Turbines and Power, 106, pp. 468-474.
[6] Camp, T. and Day, I., 1998, "A Study of Spike and Modal Stall Behavior in a Low-Speed Axial Compressor", ASME J. Turbomach., 120, pp. 393-401.
[7] Lawless, P.B. and Fleeter, S., 1993, "Rotating Stall Acoustic Signature in a Low-Speed Centrifugal Compressor: Part 2 - Vaned Diffuser", ASME Paper No. 93-GT-254.
[8] Lawless, P.B. and Fleeter, S., 1995, "Rotating Stall Acoustic Signature in a Low-Speed Centrifugal Compressor: Part 1 - Vaneless Diffuser", ASME J. Turbomach., 117, pp. 87-96.
[9] Oakes, W.C., Lawless, P.B., and Fleeter, S., 1999, "Instability Pathology of a High Speed Centrifugal Compressor," ASME Paper No. 99-GT-415.
[10] Spakovszky, Z.S. and Roduner, C.H., 2009, "Spike and Modal Stall Inception in an Advanced Turbocharger Centrifugal Compressor", ASME J. Turbomach., 131, 031012.
[11] Skoch, G.J., 2003, "Experimental Investigation of Centrifugal Compressor Stabilization Techniques," ASME Paper No. GT2003-38524.
[12] Nelson, E.B., Paduano, J.D., and Epstein, A.H., 2000, "Active Stabilization of Surge in an Axicentrifugal Turboshaft Engine", ASME J. Turbomach., vol 122, pp 485-493.
[13] Spakovszky, Z.S., 2001, "Applications of Axial and Radial Compressor Dynamic Modeling", PhD dissertation, MIT Dept. Aero/Astro.
[14] Spakovszky, Z.S., 2004, "Backward Traveling Rotating Stall Waves in Centrifugal Compressors", ASME J. Turbomach., 126, pp. 1-12.
[15] Moore, F., and Greitzer, E.M., 1986, "A Theory of Post-Stall Transients in Axial Compression Systems: Part I-Development of the Equations," ASME J. Eng. for Gas Turbines and Power, 108, pp. 68-76.
[16] Longley, J., 1994, "A Review of Nonsteady Flow Models for Compressor Stability," ASME J. Turbomach. 116, pp. 202-215.
[17] Tan, C.S., Day, I., Morris, S., and Wadia, A., 2010, "Spike-Type Compressor Stall Inception, Detection and Control," Annual Review of Fluid Mech., 42, pp. 275-300.
[18] Benneke, B., 2009, "A Methodology for Centrifugal Compressor Stability Prediction", Master's Thesis, MIT, Dept. AeroAstro.
[19] Ibaraki, S., Matsuo, T., and Yokoyama, T., 2007, "Investigation of Unsteady Flow Field in a Vaned Diffuser of a Transonic Centrifugal Compressor", ASME J. Turbomach., 129, pp. 686-693.
[20] Cukurel, B., Lawless, P.B., and Fleeter, S., 2010, "Particle Image Velocity Investigation of a High Speed Centrifugal Compressor Diffuser: Spanwise and Loading Variations," ASME J. Turbomach, 132, p. 021010.
[21] Dawes, W., 1995, "A Simulation of the Unsteady Interaction of a Centrifugal Impeller with its Vaned Diffuser: Flow Analysis", ASME J. Turbomach., 117, pp. 213-222.
[22] Shum, Y., Tan, C., and Cumpsty, N., 2000, "Impeller-Diffuser Interaction in a Centrifugal Compressor," ASME J. Turbomach., 122, pp. 777-786.
[23] Baghdadi, S., 1977, "The Effect of Rotor Blade Wakes on Centrifugal Compressor Diffuser Performance - A Comparitive Experiment", J. Fluids Engineering, 99, pp. 45-52.
[24] Everitt, J.N., 2010, "Investigation of Stall Inception in Centrifugal Compressors Using Isolated Diffuser Simulations," Master's Thesis, MIT, Dept. AeroAstro.
[25] Gould, K.A., Tan, C.S., and Macrorie, M., 2007, "Characterisation of Unsteady Impeller-Blade Loading in a Centrifugal Compressor with a Discrete-Passage Diffuser," ASME Paper No. GT2007-28002.
[26] Filipenco, V.G., Deniz, S., Johnston, J.M., Greitzer, E.M., and Cumpsty, N.A., 2000, "Effects of Inlet Flow Field Conditions on the Performance of Centrifugal Compressor Diffusers: Part 1 - Discrete-Passage Diffuser," ASME J. Turbomach., 122, pp. 1-10.
[27] Giles, M., 1989, "Non-Reflecting Boundary Conditions for Euler Equation Calculations," AIAA Journal, 28, pp. 2050-2058.
[28] Denton, J., 2010, "Some Limitations of Turbomachinery CFD," ASME Paper No. 2010-22540.
[29] Liu, Y., Liu, B., and Lu, L., 2010, "Investigation of Unsteady Impeller-Diffuser Interaction in a Transonic Centrifugal Compressor Stage," ASME Paper No. GT2010-22737.
[30] Peeters, M., and Sleiman, M, 2000, "A Numerical Investigation of the Unsteady Flow in Centrifugal Stages," ASME Paper No. 2000-GT-426.
[31] Vo, H.D., Tan, C.S., and Greitzer, E.M., 2008, "Criteria for Spike Initiated Rotating Stall," ASME J. Turbomach., 130, pp. 011023.
[32] Deppe, A., Saathof, H., and Stark, U., 2008, "Discussion: 'Criteria for Spike Initiated Rotating Stall'," ASME J. Turbomach., 130, pp. 015501.
[33] Inoue, M., Kuroumaru, M., Tanino, T., and Furukawa, M., 2000, "Propagation of Multiple Short-Length-Scale Stall Cells in an Axial Compressor Rotor," ASME J. Turbomach., 122, pp. 45-54.
[34] Inoue, M., Kuroumaru, M., Tanino, T., Yoshida, S., and Furukawa, M., 2001, "Comparative Studies on Short and Long Length-Scale Stall Cell Propagating in an Axial Compressor Rotor," ASME J. Turbomach., 123, pp. 24-32.
[35] Inoue, M., Kuroumaru, M., Yoshida, S., and Furukawa, M., 2002, "Short and Long Length-Scale Disturbances Leading to Rotating Stall in an Axial Compressor Stage With Different Stator/Rotor Gaps," ASME J. Turbomach., 124, pp. 376-384.